HOKKAIDO UNIVERSITY

Title	Effective Phonon Models Based on Symmetry-Adapted Multipole Basis — Hidden Chiral Phonon Angular Momentum Splitting in Ferroaxial Systems
Author(s)	Xie, Yu; Oiwa, Rikuto; Hayami, Satoru
Citation	Journal of the Physical Society of Japan, 95(8) https://doi.org/10.7566/JPSJ.95.083601
Issue Date	2026-08-15
Doc URL	https://hdl.handle.net/2115/100273
Rights	© 2026 The Physical Society of Japan
Type	journal article
File Information	phonon_samb_vr_black.pdf

Hokkaido University Collection of Scholarly and Academic Papers : HUSCAP

Effective phonon models based on symmetry-adapted multipole basis – Hidden chiral phonon angular momentum splitting in ferroaxial systems

Yu Xie, Rikuto Oiwa, and Satoru Hayami

Graduate School of Science, Hokkaido University, Sapporo 060-0810, Japan

We propose a symmetry-based framework for constructing effective harmonic phonon models using a symmetry-adapted multipole basis. By decomposing the force-constant matrix into bond-centered electric multipoles, we identify the minimal microscopic ingredients responsible for angular-momentum-dependent splitting of phonon dispersions. Applying this framework to a minimal zigzag-chain model, we show that ferroaxial order induces finite sublattice-resolved phonon angular momenta that cancel in the unit-cell sum. We further show that an additional polar contribution lifts this sublattice compensation, yielding a finite unit-cell-summed phonon angular momentum, thereby realizing a chiral phonon response. Our results provide a unified symmetry-based description of hidden and emergent phonon phenomena and suggest a route to control phonon properties via electronic orderings and external fields.

Chirality is characterized by the simultaneous breaking of spatial inversion $\mathcal{P}$ and mirror symmetries, and is described by a time-reversal $\mathcal{T}$-even pseudoscalar.[1] In phononic systems, chiral phonons[2–7] carrying angular momentum (AM) along the propagation vector have attracted much attention[8–13] owing to their AM-dependent dispersions and related phenomena such as phonon-induced spin polarization, electric currents, and selective optical excitation.[14–18] Ferroaxiality, by contrast, is a distinct geometric order described by a $\mathcal{T}$-even axial vector while preserving $\mathcal{P}$ symmetry.[19–21] Recent experiments and theories have identified the ferroaxial phase transition[19,22–33] and further shown the controllability of chirality through coupling to polar degrees of freedom[34,35] and emergent circular-dichroic Raman responses in centrosymmetric crystals.[36–39] Nevertheless, how ferroaxiality affects phonon dispersions remains largely unexplored. In particular, the microscopic force-constant origin of hidden sublattice-resolved phonon AM and its conversion into a finite unit-cell-summed AM by polarity remain unclear.

In this study, we construct harmonic phonon models using a symmetry-adapted multipole basis (SAMB).[40–47] This framework expands the positive-semidefinite force-constant matrix in symmetry-adapted multipoles while imposing symmetry constraints and the acoustic sum rule (ASR), enabling a unified microscopic treatment of chirality, ferroaxiality, and polarity. Applying it to a zigzag-chain model, we identify the force-constant components responsible for hidden sublattice-resolved phonon AM and show how polarity converts it into a finite unit-cell-summed AM, extending the concept of hidden textures to harmonic lattice dynamics.

Let us begin with a general formulation of effective phonon models. Within the harmonic approximation, the potential energy U is expanded up to second order in lattice displacements. Introducing the mass-weighted displacements $u_i^\alpha(\boldsymbol{R},t) = \sqrt{m_i}\, x_i^\alpha(\boldsymbol{R},t)$, where $x_i^\alpha(\boldsymbol{R},t)$ denotes the ith-sublattice atomic displacements for the $\alpha \in x,y,z$ direction ($\boldsymbol{R}$ is a Bravais lattice vector and t is the time) and m_i is the atomic mass, the energy is written as

$$U = \frac{1}{2}\sum_{\boldsymbol{R},\boldsymbol{R}'}\sum_{i,j}\sum_{\alpha,\beta} u_i^\alpha(\boldsymbol{R},t)\Phi_{ij}^{\alpha\beta}(\boldsymbol{R}-\boldsymbol{R}')u_j^\beta(\boldsymbol{R}',t), \quad (1)$$

$$\Phi_{ij}^{\alpha\beta}(\boldsymbol{R}-\boldsymbol{R}') = \frac{\partial^2 U}{\partial u_i^\alpha(\boldsymbol{R},t)\partial u_j^\beta(\boldsymbol{R}',t)}, \quad (2)$$

where $\Phi_{ij}^{\alpha\beta}(\boldsymbol{R}-\boldsymbol{R}')$ is the mass-weighted force constants. The corresponding dynamical matrix is given by

$$D_{ij}^{\alpha\beta}(\boldsymbol{q}) = \frac{1}{N}\sum_{\boldsymbol{R}}\Phi_{ij}^{\alpha\beta}(\boldsymbol{R})e^{-i\boldsymbol{q}\cdot(\boldsymbol{R}+\boldsymbol{r}_i-\boldsymbol{r}_j)}, \quad (3)$$

where N is the number of unit cells, and $\boldsymbol{r}_i$ is the position of ith-sublattice within the unit cell. The eigenvalues $\lambda_{n\boldsymbol{q}}$ and eigenvectors $\boldsymbol{\epsilon}_{n\boldsymbol{q}}$ of $\hat{D}(\boldsymbol{q})$ are obtained as $\hat{U}_{\boldsymbol{q}}^\dagger\hat{D}(\boldsymbol{q})\hat{U}_{\boldsymbol{q}} = \mathrm{diag}(\lambda_{1\boldsymbol{q}},\lambda_{2\boldsymbol{q}},\cdots,\lambda_{M\boldsymbol{q}})$ and $\hat{U}_{\boldsymbol{q}} = [\boldsymbol{\epsilon}_{1\boldsymbol{q}},\boldsymbol{\epsilon}_{2\boldsymbol{q}},\cdots,\boldsymbol{\epsilon}_{M\boldsymbol{q}}]$, from which the phonon frequencies are given by $\omega_{n\boldsymbol{q}} = \sqrt{\lambda_{n\boldsymbol{q}}}$. The displacements $\boldsymbol{u}_i(\boldsymbol{R},t)$ can then be expressed as

$$\boldsymbol{u}_i(\boldsymbol{R},t) = \frac{1}{2}\frac{1}{\sqrt{N}}\sum_{n\boldsymbol{q}}\boldsymbol{\epsilon}_{n\boldsymbol{q}}^* e^{i[\boldsymbol{q}\cdot(\boldsymbol{R}+\boldsymbol{r}_i)-\omega_{n\boldsymbol{q}}t]} + \mathrm{c.c.} \quad (4)$$

By introducing a composite index $a \equiv (i,\boldsymbol{R})$, the potential energy U can be rewritten as

$$U = \frac{1}{2}\sum_{ab}\boldsymbol{u}_a^{\mathrm{T}}\hat{\Phi}_{ab}\boldsymbol{u}_b, \quad (5)$$

where the explicit time dependence in $\boldsymbol{u}$ is omitted for simplicity. Then, the force-constant $\hat{\Phi}$ matrix satisfies:

(1) Hessian symmetry:

$$\hat{\Phi}_{ab} = \hat{\Phi}_{ba}^{\mathrm{T}}. \quad (6)$$

(2) ASR:

$$\sum_b \hat{\Phi}_{ab} = 0, \quad \hat{\Phi}_{aa} = -\sum_{b\neq a}\hat{\Phi}_{ab}. \quad (7)$$

This condition follows from translational invariance and guarantees three acoustic phonon modes with zero frequency at the Γ point. The on-site matrix elements $\hat{\Phi}_{aa}$ are fully determined by the inter-site matrix elements $\hat{\Phi}_{ab}$ ($a \neq b$) through this constraint.

(3) Positive semidefiniteness:

$$U(\{\boldsymbol{u}\}) \geq 0, \quad (8)$$

with equality only for uniform translations, ensuring me-

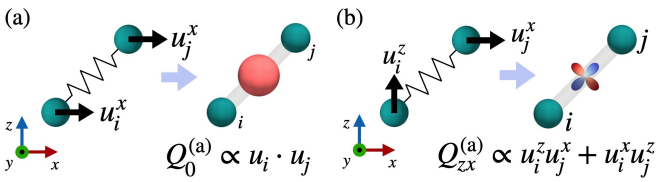

Fig. 1. (a) Schematic illustration of the force constant for the diagonal isotropic interaction, corresponding to the electric monopole $Q_0^{(a)}$ at the bond center, and (b) that for the off-diagonal anisotropic interaction, corresponding to the electric quadrupole $Q_{zx}^{(a)}$ at the bond center.

chanical stability. Equivalently, $\hat{\Phi}$ is positive semidefinite and $\hat{D}(\boldsymbol{q})$ has non-negative eigenvalues, $\omega^2(\boldsymbol{q}) \geq 0$.

We restrict ourselves to an effective harmonic model in which the energy is expressed as a sum of bond contributions depending only on relative displacements:

$$U = -\frac{1}{4}\sum_{a\neq b} \Delta\boldsymbol{u}_{ab}^{\mathrm{T}} \hat{\Phi}_{ab} \Delta\boldsymbol{u}_{ab}, \qquad \Delta\boldsymbol{u}_{ab} = \boldsymbol{u}_a - \boldsymbol{u}_b. \tag{9}$$

Such bond-based formulations are widely used in lattice dynamics for their transparent description of bond-dependent force constants and are compatibility with the mechanical stability condition (2). They have also been applied to chiral phonon systems[48,49]. In this representation, only the symmetric part $\hat{\Phi}_{ab}^{(\mathrm{S})} = \hat{\Phi}_{ab}^{(\mathrm{S})\mathrm{T}}$ contributes to the energy, since $\Delta\boldsymbol{u}_{ab}^{\mathrm{T}} \hat{\Phi}_{ab}^{(\mathrm{A})} \Delta\boldsymbol{u}_{ab} = 0$ for any antisymmetric matrix $\hat{\Phi}_{ab}^{(\mathrm{A})} = -\hat{\Phi}_{ab}^{(\mathrm{A})\mathrm{T}}$. Accordingly, we take $\hat{\Phi}_{ab}$ to be symmetric without loss of generality in this work:

$$\hat{\Phi}_{ab} = \hat{\Phi}_{ab}^{\mathrm{T}}, \quad (a \neq b). \tag{10}$$

Combining this with the Hessian symmetry in Eq. (6), we obtain

$$\hat{\Phi}_{ab} = \hat{\Phi}_{ba}, \quad (a \neq b). \tag{11}$$

Using the symmetry constraints on the force constants given by Eqs. (6), (7), (10), and (11), we show a method to construct effective harmonic phonon models based on SAMB.[40–47] Since each displacement component u^α transforms in the same way as the electronic p_α orbital, the 3×3 symmetric force constant matrix $\hat{\Phi}_{ab} = \hat{\Phi}_{ab}^{\mathrm{T}}$ for a given pair (a, b) can be described by using six electric-type atomic SAMBs:

$$\begin{aligned}
\hat{Q}_0^{(\mathrm{a})} &= \frac{1}{\sqrt{3}}\begin{pmatrix}1&0&0\\0&1&0\\0&0&1\end{pmatrix}, \hat{Q}_u^{(\mathrm{a})} = \frac{1}{\sqrt{6}}\begin{pmatrix}-1&0&0\\0&-1&0\\0&0&2\end{pmatrix}, \\
\hat{Q}_v^{(\mathrm{a})} &= \frac{1}{\sqrt{2}}\begin{pmatrix}1&0&0\\0&-1&0\\0&0&0\end{pmatrix}, \hat{Q}_{yz}^{(\mathrm{a})} = \frac{1}{\sqrt{2}}\begin{pmatrix}0&0&0\\0&0&1\\0&1&0\end{pmatrix}, \\
\hat{Q}_{zx}^{(\mathrm{a})} &= \frac{1}{\sqrt{2}}\begin{pmatrix}0&0&1\\0&0&0\\1&0&0\end{pmatrix}, \hat{Q}_{xy}^{(\mathrm{a})} = \frac{1}{\sqrt{2}}\begin{pmatrix}0&1&0\\1&0&0\\0&0&0\end{pmatrix},
\end{aligned} \tag{12}$$

where $\hat{Q}_0^{(\mathrm{a})}$ is the rank-0 electric monopole and $(\hat{Q}_u^{(\mathrm{a})}, \hat{Q}_v^{(\mathrm{a})}, \hat{Q}_{yz}^{(\mathrm{a})}, \hat{Q}_{zx}^{(\mathrm{a})}, \hat{Q}_{xy}^{(\mathrm{a})})$ are the rank-2 electric quadrupoles.

As illustrated in Fig. 1(a), $\hat{Q}_0^{(\mathrm{a})}$ corresponds to force constants that couple x–x, y–y, and z–z displacements, representing a diagonal isotropic interaction. In contrast, $\hat{Q}_{zx}^{(\mathrm{a})}$ corresponds to a force constant that couples z–x displacements, giving rise to an off-diagonal anisotropic interaction, as shown in Fig. 1(b). Although these atomic multipoles are even under $\mathcal{P}$, they can serve as the microscopic origin of AM-dependent splitting of phonon dispersions when embedded in appropriate lattice symmetry.[50,51]

Meanwhile, the remaining three antisymmetric components of the force-constant matrix under the exchange $\alpha \leftrightarrow \beta$ correspond to the atomic magnetic dipoles, given by $[M_\gamma^{(\mathrm{a})}]^{\alpha\beta} = -i\epsilon_{\alpha\beta\gamma}/\sqrt{2}$, which do not contribute to the harmonic potential U given by Eq. (9) due to the requirement in Eq. (10). Note that $\boldsymbol{M}^{(\mathrm{a})}$ is directly related to the phonon AM as[8]

$$\boldsymbol{L}^{(\mathrm{ph})} = \sqrt{2}\boldsymbol{M}^{(\mathrm{a})}. \tag{13}$$

The AM-dependent splitting of phonon dispersions discussed below can be described by writing $\boldsymbol{L}^{(\mathrm{ph})}(\boldsymbol{q})$ as an odd function of wave-vector components q_α ($\alpha = x, y, z$).

Furthermore, we introduce site- and bond-cluster SAMBs, denoted by $\hat{Y}_l^{(\mathrm{s/b})}$ ($Y = Q, T$). Here, (s) and (b) denote site- and bond-cluster quantities, respectively. The electric site- and bond-cluster SAMBs $[\hat{Q}_l^{(\mathrm{s/b})}]_{ab} = [\hat{Q}_l^{(\mathrm{s/b})}]_{ba}$ are symmetric under site exchange, whereas the magnetic-toroidal bond-cluster SAMBs $[\hat{T}_l^{(\mathrm{b})}]_{ab} = -[\hat{T}_l^{(\mathrm{b})}]_{ba}$ are antisymmetric. These quantities encode the spatial distribution and relative weight of multipoles at each site or bond, with Q and T representing the electric and magnetic toroidal multipoles, respectively. When the multipole is defined at the bond center between two sites, it is referred to as bond-cluster SAMBs.[44]

As a simple example, consider the two-site cluster shown in Fig. 1. The site-cluster SAMBs consist of the electric monopole and the electric dipole, whose 2×2 matrix representation in the sublattice basis (A, B) are given by

$$\hat{Q}_0^{(\mathrm{s})} = \frac{1}{\sqrt{2}}\begin{pmatrix}1&0\\0&1\end{pmatrix}, \hat{Q}_{\parallel}^{(\mathrm{s})} = \frac{1}{\sqrt{2}}\begin{pmatrix}1&0\\0&-1\end{pmatrix}, \tag{14}$$

where $\parallel$ means the bond-direction component between two sites. Similarly, the bond-cluster SAMBs are described by the electric monopole and magnetic toroidal dipole, which are expressed as

$$\hat{Q}_0^{(\mathrm{b})} = \frac{1}{\sqrt{2}}\begin{pmatrix}0&1\\1&0\end{pmatrix}, \hat{T}_{\parallel}^{(\mathrm{b})} = \frac{1}{\sqrt{2}}\begin{pmatrix}0&i\\-i&0\end{pmatrix}. \tag{15}$$

Because of Eq. (11), the bond-cluster magnetic toroidal SAMBs, which are antisymmetric for $a \leftrightarrow b$, $[\hat{T}_l^{(\mathrm{b})}]_{ab} = -[\hat{T}_l^{(\mathrm{b})}]_{ba}$, cannot be incorporated into the harmonic potential U.

The force constant matrix $[\hat{\Phi}]_{ab}^{\alpha\beta} = \delta_{ab}[\hat{\Phi}^{(\mathrm{on})}]_{aa}^{\alpha\beta} + (1 - \delta_{ab})[\hat{\Phi}^{(\mathrm{inter})}]_{ab}^{\alpha\beta}$ can be systematically constructed using on-site and inter-site SAMBs, denoted as blackboard-bold symbols $\hat{\mathbb{Z}}_j^{(\mathrm{on})}$ and $\hat{\mathbb{Z}}_j^{(\mathrm{inter})}$, respectively. These composite SAMBs are expressed as linear combinations of direct products between the six atomic electric SAMBs $\hat{Q}_{l_1\xi_1}^{(\mathrm{a})}$ and the site- or bond-cluster electric SAMBs $\hat{Q}_{l_2\xi_2}^{(\mathrm{s/b})}$:

$$[\hat{\mathbb{Z}}_j^{(\mathrm{on})}]_{aa}^{\alpha\beta} = \sum_{\xi_1\xi_2} C_{l\xi}^{l_1\xi_1,l_2\xi_2}(Z)[\hat{Q}_{l_1\xi_1}^{(\mathrm{a})}]^{\alpha\beta} \otimes [\hat{Q}_{l_2\xi_2}^{(\mathrm{s})}]_{aa}, \tag{16}$$

$$[\hat{\mathbb{Z}}_j^{(\mathrm{inter})}]_{ab}^{\alpha\beta} = \sum_{\xi_1\xi_2} C_{l\xi}^{l_1\xi_1,l_2\xi_2}(Z)[\hat{Q}_{l_1\xi_1}^{(\mathrm{a})}]^{\alpha\beta} \otimes [\hat{Q}_{l_2\xi_2}^{(\mathrm{b})}]_{ab}, \quad (a \neq b), \tag{17}$$

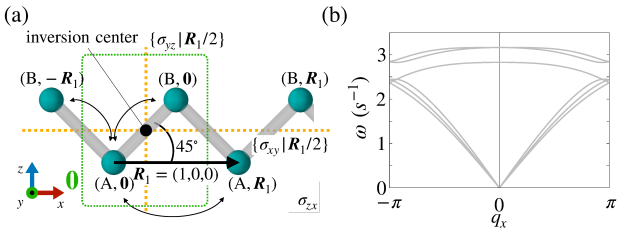

Fig. 2. (a) Schematic illustration of the one-dimensional zigzag chain. (b) Phonon energy dispersion of the model.

where $\xi = (\Gamma, n, \gamma)$, and Γ and γ denote the irreducible representation (irrep.) and its component, respectively, and the label n represents the multiplicity to distinguish independent SAMBs belonging to the same irrep. Here, we introduce the composite index $j = (Z, l, \Gamma, n, \gamma)$, where $Z = Q$ or G. For $Z = Q$ and G, we write $\hat{\mathbb{Z}}_{(Z,l,\Gamma,n,\gamma)}$ as $\hat{\mathbb{Q}}_{l\xi}$ and $\hat{\mathbb{G}}_{l\xi}$, respectively. Here, $\hat{\mathbb{Q}}_{l\xi}$ and $\hat{\mathbb{G}}_{l\xi}$ correspond to the electric and the electric toroidal composite SAMBs with $(\mathcal{P}, \mathcal{T}) = [(-1)^l, +1]$ and $[(-1)^{l+1}, +1]$, respectively. The Clebsch-Gordan (CG) coefficients $C^{l_1\xi_1, l_2\xi_2}_{l\xi}(Z)$ are normalized such that the resulting composite SAMBs form an orthonormal basis under the trace inner product.[44] The full set of SAMBs $\{\mathbb{Z}_j\}$ can be generated automatically using the Python library, `MultiPie`.[44]

Utilizing the completeness and orthonormality of the SAMBs $\{\hat{\mathbb{Z}}_j\}$, the force-constant matrix $\hat{\Phi}$ can be systematically expanded as a linear combination of $\{\hat{\mathbb{Z}}_j\}$ as

$$\begin{aligned}\hat{\Phi}^{(\mathrm{on})} &= \sum_j z_j^{(\mathrm{on})} \hat{\mathbb{Z}}_j^{(\mathrm{on})}, \quad z_j^{(\mathrm{on})} = \mathrm{Tr}\left[\hat{\mathbb{Z}}_j^{(\mathrm{on})} \hat{\Phi}^{(\mathrm{on})}\right], \\ \hat{\Phi}^{(\mathrm{inter})} &= \sum_j z_j^{(\mathrm{inter})} \hat{\mathbb{Z}}_j^{(\mathrm{inter})}, \quad z_j^{(\mathrm{inter})} = \mathrm{Tr}\left[\hat{\mathbb{Z}}_j^{(\mathrm{inter})} \hat{\Phi}^{(\mathrm{inter})}\right],\end{aligned} \tag{18}$$

where the coefficients $\{z_j^{(\mathrm{on})}\}$ and $\{z_j^{(\mathrm{inter})}\}$ serve as model parameters and are not independent, but are constrained by the AS R in Eq. (7). In particular, the on-site coefficients are determined from the inter-site ones as

$$z_i^{(\mathrm{on})} = \sum_j z_j^{(\mathrm{inter})} \sum_{a \neq b} \mathrm{Tr}\left\{[\hat{\mathbb{Z}}_i^{(\mathrm{on})}]_{aa} [\hat{\mathbb{Z}}_j^{(\mathrm{inter})}]_{ab}\right\}. \tag{19}$$

The SAMBs contributing to $\hat{\Phi}$ belong to the totally symmetric irrep. of the point group of the system. Symmetry-breaking SAMBs belonging to other irrep. can also be incorporated to analyze the effects of symmetry breaking arising from structural phase transitions or electronic orderings, as discussed below.

We demonstrate our method using a minimal one-dimensional zigzag-chain model composed of A and B sublattices [Fig. 2(a)], belonging to the space group No. 51 with point group D_{2h}. This model is particularly suitable for our purpose because, despite involving only a simple two-sublattice degree of freedom, it allows for various ordered states arising from the local breaking of $\mathcal{P}$ symmetry at each site.[52,53] The potential energy $U = (1/2) \sum_{ab}^{\mathrm{A,B}} \boldsymbol{u}_a^{\mathrm{T}} \hat{\Phi}_{ab} \boldsymbol{u}_b$ is given by

$$U = \sum_{n=1}^{2} \sum_{ab}^{\mathrm{A,B}} k^{(n)} (\Delta \boldsymbol{u}_{ab})^2 + k^{(n)'} (\boldsymbol{n}_{ab} \cdot \Delta \boldsymbol{u}_{ab})^2, \tag{20}$$

where $\boldsymbol{n}_{ab}$ is the unit vector along the bond connecting sites a and b, and $k^{(n)}$ and $k^{(n)'}$ denote the isotropic and bond-oriented

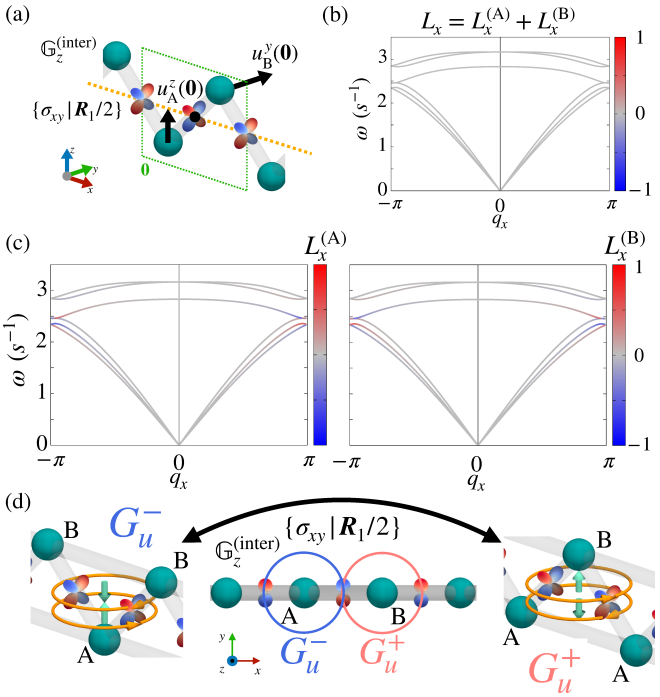

Fig. 3. (a) Schematic representation of the electric toroidal dipole $\hat{\mathbb{G}}_z^{(\mathrm{inter})}$ defined in Eq. (21), and (b) the corresponding phonon energy dispersion and AM distribution. (c) Sublattice-resolved phonon AM distribution under ferroaxial order described by $\hat{\mathbb{G}}_z^{(\mathrm{inter})}$. (d) Antiferro-type chiral order of ET quadrupoles $G_u^{\pm}$.

anisotropic force constants for the nth nearest neighbor (NN) ($n \leq 2$), respectively. In the following calculations, we set $k^{(1)} = 0.5, k^{(2)} = 0.1, k^{(1)'} = 0.25$, and $k^{(2)'} = 0.05$.

Using Eq. (18), the 6×6 force-constant matrix $\hat{\Phi}$ can be expressed as a linear combination of SAMBs belonging to the totally symmetric $\mathrm{A_g}$ irrep. as $\hat{\Phi} = \sum_j^{\Gamma_j = \mathrm{A_g}} z_j \hat{\mathbb{Z}}_j$. The resulting phonon energy dispersion obtained from this model is shown in Fig. 2(b).

We first examine the effect of ferroaxial order by introducing a SAMB corresponding to an axial vector along the z direction. The relevant term is given by

$$\hat{\mathbb{G}}_z^{(\mathrm{inter})} = \hat{Q}_{yz}^{(\mathrm{a})} \otimes \hat{Q}_{zx}^{(\mathrm{b})}, \tag{21}$$

which belongs to the $\mathrm{B_{1g}}$ irrep. Here, $\hat{Q}_{yz}^{(\mathrm{a})}$ is the atomic quadrupole matrix given by Eq. (12), whereas $\hat{Q}_{zx}^{(\mathrm{b})}$ represents the symmetry of the alternating A–B bond distribution: $[\hat{Q}_{zx}^{(\mathrm{b})}]_{\mathrm{AB}}(\boldsymbol{0}) = [\hat{Q}_{zx}^{(\mathrm{b})}]_{\mathrm{BA}}(\boldsymbol{0}) = -[\hat{Q}_{zx}^{(\mathrm{b})}]_{\mathrm{AB}}(\boldsymbol{R}_1) = -[\hat{Q}_{zx}^{(\mathrm{b})}]_{\mathrm{BA}}(-\boldsymbol{R}_1) = 1/2$. The pairs $\mathrm{AB}(\boldsymbol{0})/\mathrm{BA}(\boldsymbol{0})$ and $\mathrm{AB}(\boldsymbol{R}_1)/\mathrm{BA}(-\boldsymbol{R}_1)$ represent the same intra- and intercell A–B bonds, respectively, with opposite site ordering. Under $(\{\sigma_{xy}|\boldsymbol{R}_1/2\}, \{\sigma_{yz}|\boldsymbol{R}_1/2\}, \sigma_{zx}, \mathcal{P}, \mathcal{T})$, $\hat{Q}_{yz}^{(a)}$ and $\hat{Q}_{zx}^{(b)}$ transform as $(-1, +1, -1, +1, +1)$ and $(-1, -1, +1, +1, +1)$, respectively. Thus, their product transforms as $(+1, -1, -1, +1, +1)$, which is identical to the symmetry of the electric-toroidal dipole G_z , breaking $\{\sigma_{yz}|\boldsymbol{R}_1/2\}$ and σ_{zx}, while preserving $\{\sigma_{xy}|\boldsymbol{R}_1/2\}$, $\mathcal{P}$, and $\mathcal{T}$. Since the phonon AM is $\mathcal{P}$-even and $\mathcal{T}$-odd, whereas $\boldsymbol{q}$ is reversed by both $\mathcal{P}$ and $\mathcal{T}$, the combined $\mathcal{PT}$ symmetry keeps $\boldsymbol{q}$ invariant but reverses the phonon AM. Consequently, the unit-cell-summed phonon AM must vanish at each $\boldsymbol{q}$, as shown in Fig. 3(b).

Nevertheless, a nontrivial sublattice-resolved structure

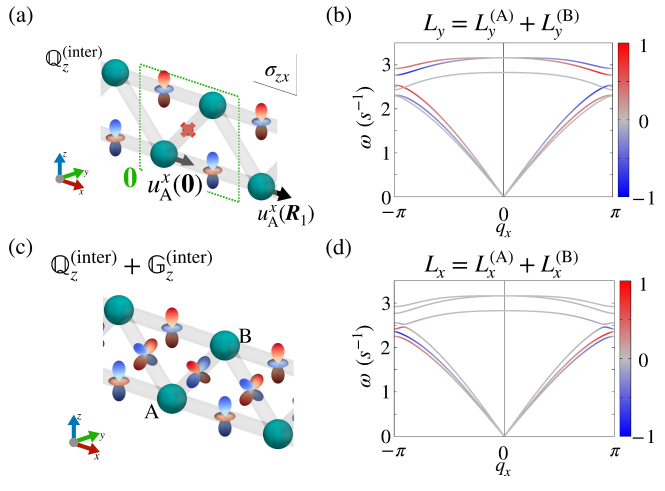

Fig. 4. (a) Schematic representation of the electric dipole $\hat{\mathbb{Q}}_z^{(\mathrm{inter})}$ defined in Eq. (22), and (b) the corresponding phonon energy dispersion with the phonon AM distribution. (c) Combined order of $\hat{\mathbb{Q}}_z^{(\mathrm{inter})}$ and $\hat{\mathbb{G}}_z^{(\mathrm{inter})}$ and (d) the corresponding phonon energy dispersion with phonon AM distribution.

emerges. As shown in Fig. 3(c), the phonon AM on each sublattice is antisymmetric in q_x, satisfying $L_x^{(\mathrm{ph}),(\mathrm{A,B})}(q_x) = -L_x^{(\mathrm{ph}),(\mathrm{A,B})}(-q_x)$. The A and B contributions have opposite signs and thus cancel in total, resulting in zero net AM. This corresponds to a hidden sublattice-resolved phonon AM, analogous to the sublattice-resolved antisymmetric spin splitting in ferroaxial electronic systems.[54] As illustrated in Fig. 3(d), this sublattice-resolved structure can be viewed as an antiferro-type arrangement of local electric-toroidal quadrupole components $G_u^{\pm}$ around the A and B sublattices. Here, G_u^- and G_u^+ are assigned to the A and B sublattices, respectively, and the signs denote opposite local chirality originating from vortex-like arrangements formed by $\hat{Q}_{yz}^{(a)}$. For each local $G_u^{\pm}$ component, $\mathcal{P}$ symmetry and all mirror symmetries with respect to the midpoint of the local quadrupole texture are broken, whereas $\mathcal{T}$ symmetry is preserved. Thus, each $G_u^{\pm}$ component has the same symmetry as a $\mathcal{T}$-even pseudoscalar chirality.

Next, we turn to a polar SAMB, in place of the ferroaxial one, corresponding to an electric polarization along the z direction. Within the SAMB framework, such a contribution is incorporated as

$$\hat{\mathbb{Q}}_z^{(\mathrm{inter})} = \hat{Q}_u^{(\mathrm{a})} \otimes \hat{Q}_z^{(\mathrm{b})}, \tag{22}$$

which belongs to the B_{1u} irrep. Here, $\hat{Q}_u^{(\mathrm{a})}$ belongs to the totally symmetric irrep., whereas $\hat{Q}_z^{(\mathrm{b})}$ transforms as the z component of a polar vector, with $-[\hat{Q}_z^{(\mathrm{b})}]_{\mathrm{AA}}(\pm\boldsymbol{R}_1) = [\hat{Q}_z^{(\mathrm{b})}]_{\mathrm{BB}}(\pm\boldsymbol{R}_1) = 1/2$. The elements $[\hat{Q}_z^{(\mathrm{b})}]_{\mathrm{AA/BB}}(\pm\boldsymbol{R}_1)$ represent same-sublattice intercell bonds. In the polar state, σ_{zx} is preserved. Along the q_x line, q_x is invariant under σ_{zx}, whereas the axial phonon AM transforms as $(L_x^{(\mathrm{ph})}, L_y^{(\mathrm{ph})}, L_z^{(\mathrm{ph})}) \to (-L_x^{(\mathrm{ph})}, L_y^{(\mathrm{ph})}, -L_z^{(\mathrm{ph})})$. Thus, $L_x^{(\mathrm{ph})}$ and $L_z^{(\mathrm{ph})}$ are forbidden along the q_x line, while $L_y^{(\mathrm{ph})}$ is allowed. $\mathcal{T}$ symmetry further imposes $L_y^{(\mathrm{ph})}(q_x) = -L_y^{(\mathrm{ph})}(-q_x)$. The corresponding phonon dispersion exhibits a Rashba-type antisymmetric splitting of the phonon AM, as shown in Fig. 4(b).

We then consider the combined effect of the ferroaxial and polar SAMBs. As shown in Fig. 4(c), introducing both $\hat{\mathbb{G}}_z^{(\mathrm{inter})}$ and $\hat{\mathbb{Q}}_z^{(\mathrm{inter})}$ breaks all mirror symmetries as well as $\mathcal{P}$ symmetry, thereby realizing a chiral system. In the ferroaxial state alone, the sublattice-resolved chiral components $G_u^{\pm}$ cancel due to the remaining mirror symmetry σ_{xy}. However, once the polar term is introduced, this symmetry is lifted, rendering the A and B sublattices inequivalent. As a result, the cancellation of local chirality is removed, and a finite global chirality emerges. This is clearly reflected in the phonon AM distribution shown in Fig. 4(d), where a net antisymmetric component of $L_x^{(\mathrm{ph})}$ develops along the q_x line.

Finally, we discuss the minimal microscopic model parameters responsible for the characteristic AM-dependent splitting of phonon dispersions. For the ferroaxial case, the hidden sublattice-resolved splitting $L_x^{(\mathrm{ph}),(\mathrm{A,B})}$ already appears with the NN isotropic force constant $k^{(1)}$ in U given by Eq. (20). In contrast, the polarization-induced splitting $L_y^{(\mathrm{ph})}$ requires both $k^{(1)}$ and $k^{(1)'}$, reflecting the necessity of an additional NN off-diagonal component. When both ferroaxiality and polarity are present, a chiral AM-dependent splitting emerges with $k^{(1)}$ alone, without requiring additional off-diagonal force constants.

We developed a symmetry-based framework for constructing effective harmonic phonon models using the SAMB. By decomposing the force-constant matrix under symmetry constraints and the ASR, we identified the minimal ingredients responsible for AM-dependent splitting. Applying this framework to a minimal zigzag-chain model, we show that a ferroaxial SAMB generates hidden sublattice-resolved phonon AM that cancels globally due to $\mathcal{P}$ and $\mathcal{T}$ symmetries. Introducing a polar SAMB lifts this cancellation by breaking inversion and mirror symmetries, leading to a chiral phonon dispersion. Thus, the interplay of ferroaxiality and polarity converts hidden chirality into observable phonon responses. Our results provide a unified symmetry-adapted description of AM-dependent splitting across ferroaxial, polar, and chiral systems, and offer a systematic route to designing phononic responses via symmetry breaking.

Acknowledgment The authors thank H. Kusunose for fruitful discussions. This research was supported by JSPS KAKENHI Grants Numbers JP22H00101, JP23H04869, and by JST CREST (JPMJCR23O4) and JST FOREST (JPMJFR2366).

1) L. D. Barron: Rend. Lincei Sci. Fis. Nat. **24** (2013) 179.
2) H. Zhu, J. Yi, M.-Y. Li, J. Xiao, L. Zhang, C.-W. Yang, R. A. Kaindl, L.-J. Li, Y. Wang, and X. Zhang: Science **359** (2018) 579.
3) H. Chen, W. Wu, J. Zhu, Z. Yang, W. Gong, W. Gao, S. A. Yang, and L. Zhang: Nano Letters **22** (2022) 1688.
4) E. Bousquet, M. Fava, Z. Romestan, F. Gómez-Ortiz, E. E. McCabe, and A. H. Romero: Journal of Physics: Condensed Matter **37** (2025) 163004.
5) A. Kato and J.-i. Kishine: J. Phys. Soc. Jpn. **92** (2023) 075002.
6) T. Wang, H. Sun, X. Li, and L. Zhang: Nano Letters **24** (2024) 4311.
7) D. M. Juraschek, R. M. Geilhufe, H. Zhu, M. Basini, P. Baum, A. Baydin, S. Chaudhary, M. Fechner, B. Flebus, G. Grissonnanche, A. I. Kirilyuk, M. Lemeshko, S. F. Maehrlein, M. Mignolet, S. Murakami, Q. Niu, U. Nowak, C. P. Romao, H. Rostami, T. Satoh, N. A. Spaldin, H. Ueda, and L. Zhang: Nature Physics **21** (2025) 1532.
8) L. Zhang and Q. Niu: Phys. Rev. Lett. **112** (2014) 085503.
9) L. Zhang and Q. Niu: Phys. Rev. Lett. **115** (2015) 115502.
10) Y. Tatsumi, T. Kaneko, and R. Saito: Phys. Rev. B **97** (2018) 195444.
11) T. Zhang and S. Murakami: Phys. Rev. Res. **4** (2022) L012024.
12) H. Komiyama, T. Zhang, and S. Murakami: Phys. Rev. B **106** (2022) 184104.

13) H. Zhang, N. Peshcherenko, F. Yang, T. Ward, P. Raghuvanshi, L. Lindsay, C. Felser, Y. Zhang, J. Yan, and H. Miao: Nat. Phys. **21** (2025) 1387.
14) A. S. PINE and G. DRESSELHAUS: Phys. Rev. **188** (1969) 1489.
15) K. Ishito, H. Mao, Y. Kousaka, Y. Togawa, S. Iwasaki, T. Zhang, S. Murakami, J.-i. Kishine, and T. Satoh: Nat. Phys. **19** (2023) 35.
16) K. Ishito, H. Mao, K. Kobayashi, Y. Kousaka, Y. Togawa, H. Kusunose, J.-i. Kishine, and T. Satoh: Chirality **35** (2023) 338.
17) E. Oishi, Y. Fujii, and A. Koreeda: Phys. Rev. B **109** (2024) 104306.
18) H. Ueda, M. García-Fernández, S. Agrestini, C. P. Romao, J. van den Brink, N. A. Spaldin, K.-J. Zhou, and U. Staub: Nature **618** (2023) 946.
19) W. Jin, E. Drueke, S. Li, A. Admasu, R. Owen, M. Day, K. Sun, S.-W. Cheong, and L. Zhao: Nat. Phys. **16** (2020) 42.
20) J. Hlinka: Phys. Rev. Lett. **113** (2014) 165502.
21) J. Hlinka, J. Privratska, P. Ondrejkovic, and V. Janovec: Phys. Rev. Lett. **116** (2016) 177602.
22) R. Owen, E. Drueke, C. Albunio, A. Kaczmarek, W. Jin, D. Obeysekera, S.-W. Cheong, J. Yang, S. Cundiff, and L. Zhao: Phys. Rev. B **103** (2021) 054104.
23) T. Hayashida, Y. Uemura, K. Kimura, S. Matsuoka, D. Morikawa, S. Hirose, K. Tsuda, T. Hasegawa, and T. Kimura: Nat. Commun. **11** (2020) 4582.
24) T. Hayashida, Y. Uemura, K. Kimura, S. Matsuoka, M. Hagihala, S. Hirose, H. Morioka, T. Hasegawa, and T. Kimura: Phys. Rev. Materials **5** (2021) 124409.
25) H. Yokota, T. Hayashida, D. Kitahara, and T. Kimura: npj Quantum Mater. **7** (2022) 106.
26) X. Fang, C. De, F.-T. Huang, X. Xu, K. Du, K. Wang, B. Li, and S.-W. Cheong: J. Am. Chem. Soc. **145** (2023) 28022.
27) X. Guo, R. Owen, A. Kaczmarek, X. Fang, C. De, Y. Ahn, W. Hu, N. Agarwal, S. H. Sung, R. Hovden, S.-W. Cheong, and L. Zhao: Phys. Rev. B **107** (2023) L180102.
28) T. Hasegawa, W. Yoshida, K. Nakamura, N. Ogita, and K. Matsuhira: J. Phys. Soc. Jpn. **89** (2020) 054602.
29) H. Hanate, T. Hasegawa, S. Hayami, S. Tsutsui, S. Kawano, and K. Matsuhira: J. Phys. Soc. Jpn. **90** (2021) 063702.
30) H. Hanate, S. Tsutsui, T. Yajima, H. Nakao, H. Sagayama, T. Hasegawa, and K. Matsuhira: J. Phys. Soc. Jpn. **92** (2023) 063601.
31) S. Hayami, S. Tsutsui, H. Hanate, N. Nagasawa, Y. Yoda, and K. Matsuhira: J. Phys. Soc. Jpn. **92** (2023) 033702.
32) S. Yamagishi, T. Hayashida, R. Misawa, K. Kimura, M. Hagihala, T. Murata, S. Hirose, and T. Kimura: Chem. Mater. **35** (2023) 747.
33) Y. Xie, R. Oiwa, and S. Hayami: Phys. Rev. B **113** (2026) 205133.
34) T. Hayashida, K. Kimura, and T. Kimura: Proceedings of the National Academy of Sciences **120** (2023) e2303251120.
35) S. Hayami, R. Oiwa, and A. Inda: J. Phys. Soc. Jpn. **94** (2025) 123702.
36) H. Watanabe, R. Oiwa, G. Kusuno, T. Satoh, and R. Arita: Phys. Rev. B **112** (2025) 115105.
37) G. Kusuno, T. Hayashida, T. Nagai, H. Watanabe, R. Oiwa, T. Kimura, and T. Satoh: Phys. Rev. Lett. (2026) .
38) H. Watanabe, R. Oiwa, H. Mori, and R. Arita: arXiv:2507.09237 (2026).
39) Y. Suganuma, G. Kusuno, H. Watanabe, R. Oiwa, H. Mori, R. Arita, and T. Satoh: arXiv:2603.21756 (2026).
40) S. Hayami, M. Yatsushiro, Y. Yanagi, and H. Kusunose: Phys. Rev. B **98** (2018) 165110.
41) H. Kusunose, R. Oiwa, and S. Hayami: J. Phys. Soc. Jpn. **89** (2020) 104704.
42) S. Hayami and H. Kusunose: J. Phys. Soc. Jpn. **93** (2024) 072001.
43) R. Oiwa and H. Kusunose: Phys. Rev. Lett. **129** (2022) 116401.
44) H. Kusunose, R. Oiwa, and S. Hayami: Phys. Rev. B **107** (2023) 195118.
45) A. Inda, R. Oiwa, S. Hayami, H. M. Yamamoto, and H. Kusunose: The Journal of Chemical Physics **160** (2024) 184117.
46) R. Oiwa and H. Kusunose: Phys. Rev. Res. **7** (2025) 033250.
47) R. Oiwa, A. Inda, S. Hayami, T. Nomoto, R. Arita, and H. Kusunose: Phys. Rev. B **112** (2025) 035116.
48) H. Tsunetsugu and H. Kusunose: J. Phys. Soc. Jpn. **92** (2023) 023601.
49) H. Tsunetsugu and H. Kusunose: J. Phys. Soc. Jpn. **95** (2026) 013601.
50) S. Hayami, Y. Yanagi, H. Kusunose, and Y. Motome: Phys. Rev. Lett. **122** (2019) 147602.
51) T. Ishitobi and K. Hattori: Phys. Rev. Lett. **136** (2026) 056402.
52) Y. Yanase: J. Phys. Soc. Jpn. **83** (2014) 014703.
53) S. Hayami, H. Kusunose, and Y. Motome: J. Phys.: Condens. Matter **28** (2016) 395601.
54) S. Bhowal and N. A. Spaldin: Phys. Rev. Res. **6** (2024) 043141.